Stanford Exploration Project, Report 72, December 18, 1997, pages 1–112

Short Note

Accurate, efficient 2-D elastic modeling using S&M

Carlos A. Cunha Filho[1]

keywords: *modeling, elastic, two-dimensional*

INTRODUCTION

Some important aspects of accurate finite-difference elastic modeling algorithms are the use of high order differential operators, staggered grid computations, and a two-step implementation of the spatial operator by first obtaining the strains and then the stresses (Dablain, 1986; Mora, 1986; Etgen, 1989). The high-order operators are required to avoid numerical anisotropy and dispersion, while the staggered scheme is important to guarantee the spatial synchronization of the two-step 1-D operators used in the strain-stress implementation. Using the exact solution of a discrete physical system (Cunha, 1991) as guide for the discretization, and following the equivalence relations defined in the algebra of Shoenberg and Muir (1989), I have derived an alternative one-step scheme, which avoids the intermediate computation of strains and does not require the use of the staggered grid for its implementation. The decoupling in the computations of the spatial derivatives of *fields* and *elastic parameters* obtained with this scheme allows the use of operators of different size (order). This is particularly important for modeling*blocky* models in which two-point operators aree more appropriate for computing the derivatives of the elastic constants than large operators.

THEORY

The basis for discretization

Let's consider the 1-D elastic system shown in Figure **??**, which can either represent a discrete system or the discrete representation of a continuous system. Differently from the system in Cunha (1991), this system represents the masses and springs as a

[1]**email:** not available

single entity. In the case of a discrete system, the equation of motion for point i is

$$\Delta x^2 \rho_i \frac{\partial^2 u_i}{\partial t^2} = \hat{Y}_{i-1} u_{i-1} - (\hat{Y}_{i-1} + \hat{Y}_{i+1}) u_i + \hat{Y}_{i+1} u_{i+1}, \tag{1}$$

where

$$\begin{aligned} \hat{Y}_{i-1} &= 2\frac{Y_{i-1}Y_i}{Y_{i-1}+Y_i} \\ \hat{Y}_{i+1} &= 2\frac{Y_{i+1}Y_i}{Y_{i+1}+Y_i} \end{aligned} \tag{2}$$

are the equivalent Young moduli that control the interaction between adjacent units of the system.

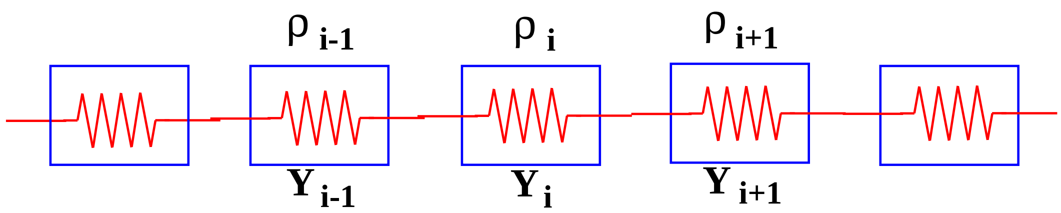

Figure 1: A mass-spring model that can represent either a discrete physical system or the discretization of a continuous elastic system. carlos3-spring2 [NR]

On the other hand, if we consider the system as continuous, the continuous equation to be discretized is

$$\rho \frac{\partial^2 u}{\partial t^2} = \frac{\partial Y \frac{\partial u}{\partial x}}{\partial x} = \frac{\partial Y}{\partial x}\frac{\partial u}{\partial x} + Y\frac{\partial^2 u}{\partial x^2}. \tag{3}$$

Two important related issues come up in the discretization of (3): the definition of the appropriate Y to use in each of the terms of the equation, and the choice of the differential star for the first-order derivative. If we choose the more precise $(-1, 1)$ star, the two terms of equation (3) will not be centered at the same point, while the star $(-.5, 0, .5)$ will not have the same resolution. Looking into the physics of the process gives a clue for the correct choice of Y; it is the one that is actually involved in the interaction between adjacent points (the equivalent Young modulus). It turns out that this choice also solves the problem of the differential star. Using this criterion, the discretization of (3) leads to

$$\begin{aligned} \rho_i \frac{\partial^2 u_i}{\partial t^2} &= \frac{(\hat{Y}_{i+1} - \hat{Y}_{i-1})}{\Delta x}\frac{(u_{i+1} - u_{i-1})}{2\Delta x} + \frac{(\hat{Y}_{i-1} + \hat{Y}_{i+1})}{2}\left(\frac{u_{i-1} - 2u_i + u_{i+1}}{\Delta x^2}\right) \\ \Delta x^2 \rho_i \frac{\partial^2 u_i}{\partial t^2} &= \hat{Y}_{i-1} u_{i-1} - (\hat{Y}_{i-1} + \hat{Y}_{i+1}) u_i + \hat{Y}_{i+1} u_{i+1}, \end{aligned}$$

which is identical to equation (1).

Using equation (1) as the basis for the discretization process offers some advantages over the usual methods. The differential operator can be applied in a single stage (without the intermediate evaluation of strain components), allowing for the design of a more efficient algorithm. In addition, the differentiation of the model parameters is completely separated from the differentiation of the wavefield components, and since the model parameters do not change with time their derivatives need to be computed only once. This independence of the derivatives of the elastic constants relative to the wavefield has an extra advantage when a *blocky model* (one with sharp boundaries) is to be modeled. In such models, a short two-point operator can be used for the elastic derivatives since *large operators will not give the right answer at the boundaries because blocky models are aliased.* Finally, the operation can be implemented in a non-staggered grid, since it is executed in one stage and all derivatives are centered.

The Shoenberg-Muir equivalence

For the case of a 2-D elastic medium, the relations for finding the equivalent 1D Young modulus (equation (2)) needs to be extended for all the involved 2-D elastic moduli. This extension is provided by the group theory of Shoenberg and Muir (1989), which defines the equations for finding the equivalent elastic parameters.

The general elastic wave equation is given by

$$\rho\frac{\partial^2 u_i}{\partial t^2} - f_i = \frac{\partial \tau_{ij}}{\partial x_j}, \tag{4}$$

where indices i and j refers to the spatial components (x, y, z), f_i is the i component of the internal forces, and τ_{ij} is the ij component of the stress field (Auld, 1990). In the 2-D transverse isotropic case without internal sources, the x component of equation (4) becomes

$$\rho\frac{\partial^2 u_x}{\partial t^2} = \frac{\partial \tau_{xx}}{\partial x} + \frac{\partial \tau_{xz}}{\partial z},$$

where

$$\tau_{xx} = c_{11}\frac{\partial u_x}{\partial x} + c_{13}\frac{\partial u_z}{\partial z}, \qquad \text{and} \qquad \tau_{xz} = c_{55}\left(\frac{\partial u_x}{\partial z} + \frac{\partial u_z}{\partial x}\right).$$

Combining these equations we find for the x component

$$\begin{aligned}\rho\frac{\partial^2 u_x}{\partial t^2} = {} & \frac{\partial \hat{c}_{11}}{\partial x}\frac{\partial u_x}{\partial x} + \hat{c}_{11}\frac{\partial^2 u_x}{\partial x^2} + \frac{\partial \hat{c}_{13}}{\partial x}\frac{\partial u_z}{\partial z} + \hat{c}_{13}\frac{\partial^2 u_z}{\partial x \partial z} \\ & + \frac{\partial \hat{c}_{55}}{\partial z}(\frac{\partial u_x}{\partial z} + \frac{\partial u_z}{\partial x}) + \hat{c}_{55}(\frac{\partial^2 u_x}{\partial z^2} + \frac{\partial^2 u_z}{\partial x \partial z}),\end{aligned} \tag{5}$$

and for the z component

$$\begin{aligned}\rho\frac{\partial^2 u_z}{\partial t^2} = {} & \frac{\partial \hat{c}_{33}}{\partial z}\frac{\partial u_z}{\partial z} + \hat{c}_{33}\frac{\partial^2 u_z}{\partial z^2} + \frac{\partial \hat{c}_{13}}{\partial z}\frac{\partial u_x}{\partial x} + \hat{c}_{13}\frac{\partial^2 u_x}{\partial z \partial x} \\ & + \frac{\partial \hat{c}_{55}}{\partial x}(\frac{\partial u_z}{\partial x} + \frac{\partial u_x}{\partial z}) + \hat{c}_{55}(\frac{\partial^2 u_z}{\partial x^2} + \frac{\partial^2 u_x}{\partial z \partial x}).\end{aligned} \tag{6}$$

The equivalent stiffness constants $\hat{c}$ are obtained with the Shoenberg-Muir algebra. For displacements in the x direction,

$$\begin{aligned}
\hat{c}_{11}^{ij} &= \frac{2c_{11}^{i}c_{11}^{j}}{c_{11}^{i}+c_{11}^{j}} \\
\hat{c}_{55}^{ij} &= \frac{2c_{55}^{i}c_{55}^{j}}{c_{55}^{i}+c_{55}^{j}} \\
\hat{c}_{13}^{ij} &= \frac{\hat{c}_{11}^{ij}}{2}\left(\frac{c_{13}^{i}}{c_{11}^{i}}+\frac{c_{13}^{j}}{c_{11}^{j}}\right)
\end{aligned} \tag{7}$$

and for displacements in the z direction,

$$\begin{aligned}
\hat{c}_{33}^{ij} &= \frac{2c_{33}^{i}c_{33}^{j}}{c_{33}^{i}+c_{33}^{j}} \\
\hat{c}_{55}^{ij} &= \frac{2c_{55}^{i}c_{55}^{j}}{c_{55}^{i}+c_{55}^{j}} \\
\hat{c}_{13}^{ij} &= \frac{\hat{c}_{33}^{ij}}{2}\left(\frac{c_{13}^{i}}{c_{33}^{i}}+\frac{c_{13}^{j}}{c_{33}^{j}}\right).
\end{aligned} \tag{8}$$

IMPLEMENTATION

Absorbing boundaries

The absorbing boundary conditions in the sides and bottom of the model are based in the method described by Cerjan et al. (1985), which is at the same time simple and suitable for implementation in a parallel architecture. An N-grid-points-thick absorbing region covers the three absorbing regions. Following each time step, the wavefield inside this region is multiplied by a Gaussian damping function $G = \exp -[(N-i)/\sigma_N]^2$., where i is the distance (in grid-points units) from the boundary. The total attenuation applied to a wavefield propagating with an extreme velocity of one grid-point per time-step is

$$\Psi(t+2N\Delta t) = \prod_{i=1}^{N} G^2(i), \tag{9}$$

as illustrated in Figure **??**. Stable modeling requires velocities smaller than that, resulting in a cumulative attenuation always stronger than that described by equation (9). One of the nice things about the parallel architecture is the facility provided by the natural circular boundary conditions. No special treatment is required for the two sides of the model because the waves transmitted from one boundary to the other are sufficiently attenuated to have any significant effect.

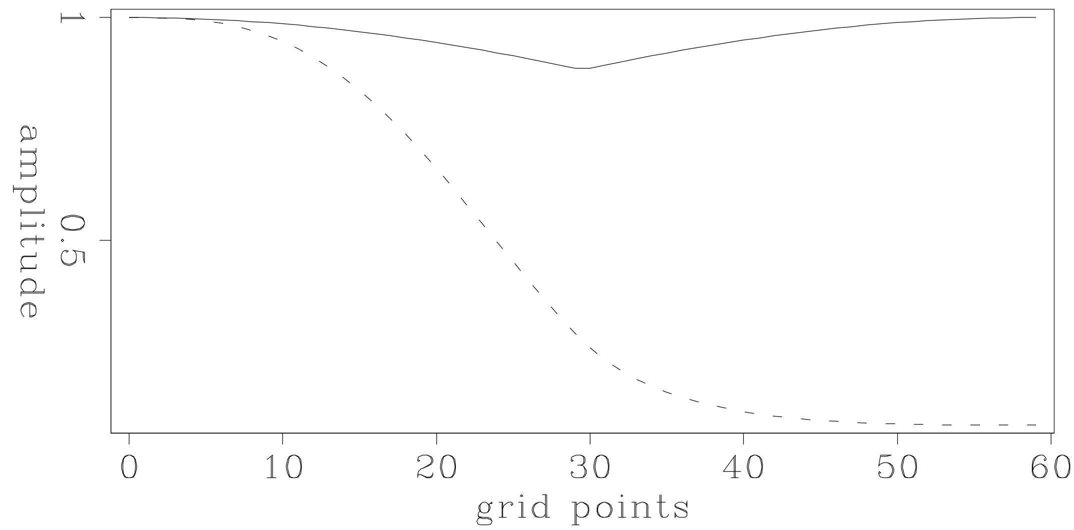

Figure 2: The continuous curve represents the attenuation applied at each grid point inside the absorbing region, while the dashed line represents the cumulative attenuation suffered by a wavefield propagating with a velocity of one-gridpoint per time-step as described by equation (**??**). carlos3-absorbing [ER]

The free boundary and the source term

The upper boundary is considered as a perfect mirror that simulates a free boundary condition. It is necessary to consider two factors in this simulation: how to apply the spatial operators at grid-points closer to the surface than the half-size of the operators, and how to define the source term.

When applied to the grid-points near the surface, the spatial operators are folded back (reflected) in the following way: The part of the operator that operates in the z component of the wavefield retains its original polarity, while the part that operates in the x component has its polarity reversed (see Figure **??**-a).

The source term is introduced as an additive contribution to the wavefield at the source location, during the time span in which the source is considered active. To avoid spatial aliasing (and also to allow the definition of a pressure source) the source needs to be spatially smooth, that is, covering a determined region of space. When the source is located sufficiently close to the surface (as is usually the case in the real world) the free-surface image of the source will be also active in the bottom space where the model is defined, as Figure **??**-b shows. Therefore, the source term needs to be introduced as the sum of the contributions of the *real* source and of its *image* in the model space region.

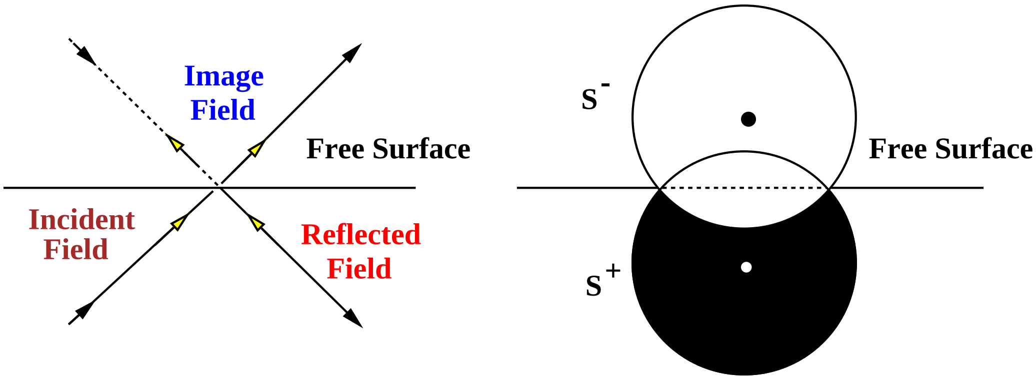

Figure 3: The free surface boundary can be replaced by an image medium and an image source. *(a)* The image wavefield has the same amplitude and reverse horizontal polarity as the object field. The black arrow represents the propagation direction; the white arrow the polarization direction. *(b)* The image source also has reverse horizontal polarity and will only be effective in the modeling if located sufficiently close to the boundary. carlos3-fresurf [NR]

The temporal and spatial operators

The spatial operator was designed to be grid-centered of eighth order (9 points). It can be decomposed in three parts for each component:

$$\mathbf{Au} \;=\; \begin{bmatrix} \mathbf{c_x} & (\mathbf{a_x}+\mathbf{b_x}) \\ (\mathbf{a_z}+\mathbf{b_z}) & \mathbf{c_z} \end{bmatrix} \begin{pmatrix} u_x \\ u_z \end{pmatrix}, \tag{10}$$

where

$$\begin{aligned}
\mathbf{a_x} &= \frac{(\hat{c}_{13}+\hat{c}_{55})}{\rho\Delta x\Delta z}\delta^2_{xz} \qquad \mathbf{b_x} = \frac{(\delta_x\hat{c}_{13}\delta_z+\delta_z\hat{c}_{55}\delta_x)}{\rho\Delta x\Delta z} \\
\mathbf{c_x} &= \frac{(\hat{c}_{11}\delta^2_{xx}+\delta_x\hat{c}_{11}\delta_x)}{\rho(\Delta x)^2}+\frac{(\hat{c}_{55}\delta^2_{zz}+\delta_z\hat{c}_{55}\delta_z)}{\rho(\Delta z)^2} \\
\mathbf{a_z} &= \frac{(\hat{c}_{13}+\hat{c}_{55})}{\rho\Delta x\Delta z}\delta^2_{xz} \qquad \mathbf{b_z} = \frac{(\delta_z\hat{c}_{13}\delta_x+\delta_x\hat{c}_{55}\delta_z)}{\rho\Delta x\Delta z} \\
\mathbf{c_z} &= \frac{(\hat{c}_{33}\delta^2_{zz}+\delta_z\hat{c}_{33}\delta_z)}{\rho(\Delta z)^2}+\frac{(\hat{c}_{55}\delta^2_{xx}+\delta_x\hat{c}_{55}\delta_x)}{\rho(\Delta x)^2}.
\end{aligned} \tag{11}$$

a and **b** are antisymmetric but **c** has no particular symmetry (except in homogeneous media); and their form is represented in Figure **??**. The δ operators are grid-centered, normalized, bi-dimensional difference stars.

The temporal updating uses the operator $\mathbf{P}^+$ described in Cunha (1991) in this report. To obtain the wavefield and its time derivative at time time $t+\Delta t$ only requires information from time t, that is,

$$\begin{pmatrix} \mathbf{u} \\ \dot{\mathbf{u}} \end{pmatrix}_{t+dt} \approx \mathbf{P}_+ \begin{pmatrix} \mathbf{u} \\ \dot{\mathbf{u}} \end{pmatrix}_t ,$$

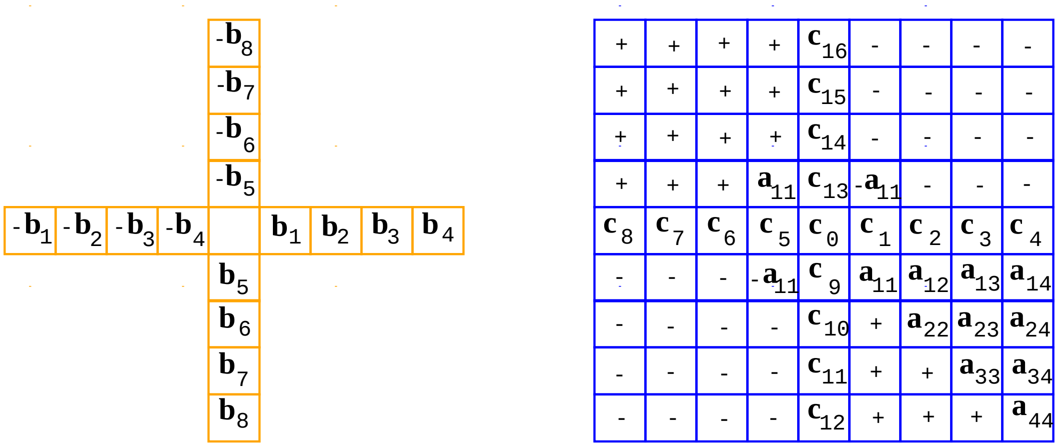

Figure 4: Spatial difference operators described by equation (11). carlos3-spaceop [NR]

where the forward time-propagation operator $\mathbf{P}_+$ has the form

$$\mathbf{P}_+ = \begin{bmatrix} \mathbf{I} + \frac{\mathbf{A}}{2}dt^2 + \frac{\mathbf{A}^2}{24}dt^4 & \mathbf{I}dt + \frac{\mathbf{A}}{6}dt^3 \\ \mathbf{A}\left(\mathbf{I}dt + \frac{\mathbf{A}}{6}dt^3\right) & \mathbf{I} + \frac{\mathbf{A}}{2}dt^2 + \frac{\mathbf{A}^2}{24}dt^4 \end{bmatrix}, \tag{12}$$

which represents a fourth order approximation in time.

EXAMPLES

In this section I show two examples that illustrate the method. The first one represents a vertically polarized displacement source in a two-layer medium (Figure **??**). The top medium is isotropic and the bottom medium (where the source is located) is transverse-isotropic. Both the vertical and horizontal components of the displacement field are displayed.

The second example (Figure **??**) has an explosive source located below a free-surface boundary. The media has some degree of structural complexity and the side and bottom boundaries are absorbing, with the absorbing region visible in the figure.

CONCLUSIONS

Using a discrete physical system as a guide for discretizing the wave equation, I have derived an alternative 2-D transverse-isotropic modeling scheme that might provide more accurate wavefield simulations for *blocky-like* models than the usual stress-strain methods. This scheme uses equivalent medium theory to construct a bridge between differential and difference equations. The method was implemented efficiently in a parallel architecture using spatial differential operators of different orders depending

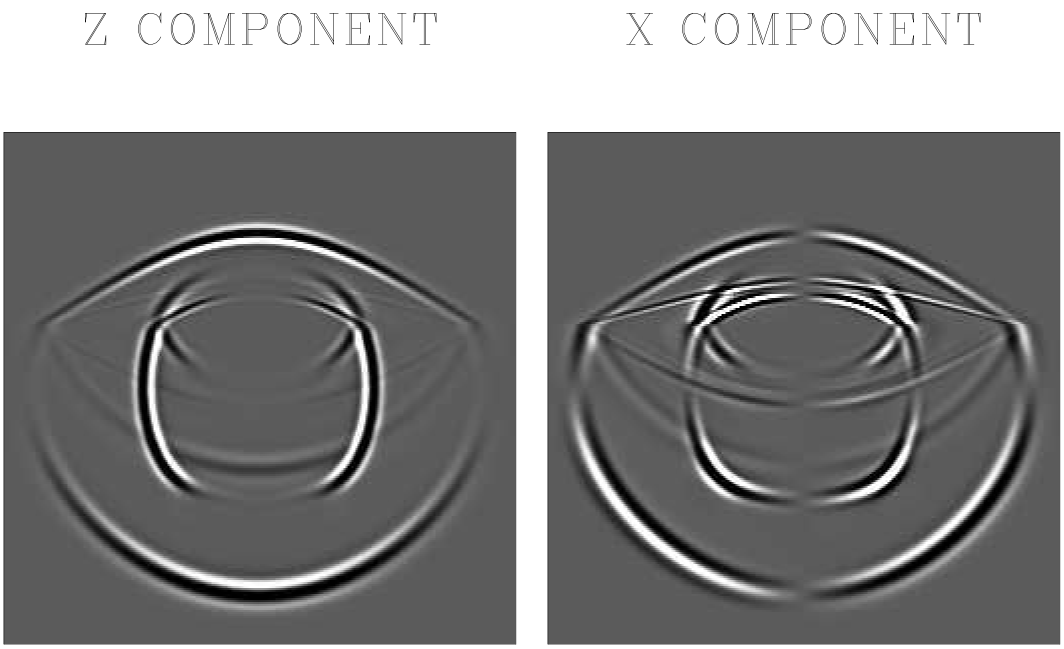

Figure 5: The source is a vertically-polarized displacement field located in the bottom layer of a two-layer model. The upper layer is isotropic, while the bottom is transverse isotropic. The left and right panels represent, respectively, the vertical and the horizontal components of the displacement field. Press the button to see a movie. carlos3-elastic1 [ER]

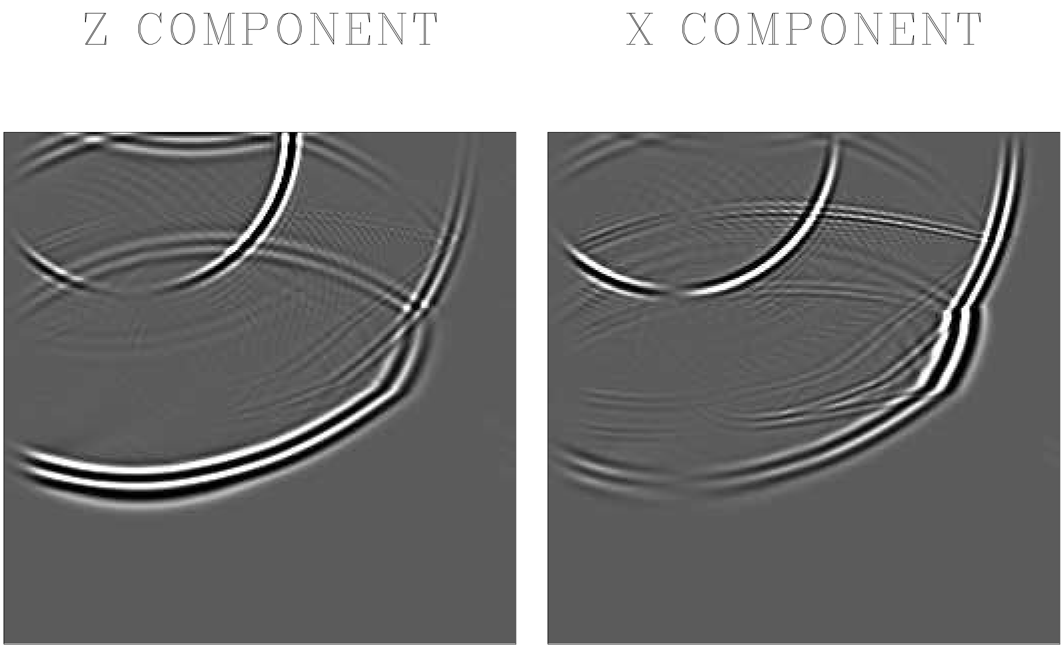

Figure 6: The source is a spherically symmetric explosive field located near the free surface of a structurally complex model. The two panels follow the same convention as Figure (**??**). Press the button to see a movie. carlos3-elastic2 [ER]

on whether they are applied to wavefields or elastic parameters. Two examples show the results of the application of this modeling scheme to physical models with distinct characteristics. These results illustrate the stability and accuracy of the method.

REFERENCES

Auld, B.A. , 1990, Acoustic fields and waves in solids, vol. I: Second edition, Krieger Publishing Company, 142–145.

Cerjan, C., Kosloff, D., Kosloff, R., and Reshef, M., 1985, A nonreflecting boundary condition for discrete acoustic and elastic wave equations: Geophysics, **50**, 705–708.

Cunha, C.A., 1991, Modeling a discrete system by eigenvalue decomposition: SEP–**72**, 55–71.

Dablain, M.A., 1986, The application of high-order differencing to the scalar wave equation: Geophysics, **51**, 54–66.

Etgen, J.T., 1989, Accurate wave equation modeling: SEP–**60**, 131–147.

Mora, P., 1986, Elastic finite-differences with convolutional operators: SEP–**48**, 151–169.

Shoenberg, M., and Muir, F., 1989, A calculus for finely layered anisotropic media: Geophysics, **54**, 581–589.